Southern Ocean mean state constrains historical warming via radiative forcing and evaporative damping

Yiqun Tian[1], Shineng Hu[1,2*], Clara Deser[3], Xianglei Huang[4], Xiuhong Chen[4]

[1] *Division of Earth and Climate Sciences, Nicholas School of the Environment, Duke University, Durham, NC, USA*

[2] *Department of Civil and Environmental Engineering, Pratt School of Engineering, Duke University, Durham, NC, USA*

[3] *Climate and Global Dynamics, National Center for Atmospheric Research, Boulder, CO, USA*

[4] *Department of Climate and Space Sciences and Engineering, the University of Michigan, Ann Arbor, MI, USA*

[*] Corresponding author: Shineng Hu (shineng.hu@duke.edu)

Abstract

Large uncertainties in equilibrium climate sensitivity (ECS) and transient climate response (TCR) have persisted for several decades and are linked to discrepancies in historical warming rate across models. Analyzing 754 historical simulations of 30 Coupled Model Intercomparison Project 6 (CMIP6) models, including 12 Large-Ensemble (LE) models, we identify the Southern Ocean (SO) climatological sea surface temperature (SST) as one potential source of inter-model spread in the twentieth-century warming. Models with a colder SO tend to simulate significantly stronger SO and global warming trends. This negative correlation results from CO_2-induced surface longwave radiative forcing modulated by climatological precipitable water and from warming-induced evaporative damping modulated by climatological latent heat flux. These two mechanisms, mainly the evaporative damping, explain 70% of the inter-model spread in the SO warming. Our findings highlight the need to reduce the model bias and spread in SO climatological SST to better constrain anthropogenic SO and global warming.

Main

ECS and TCR are two key metrics of climate sensitivity quantifying the global mean surface temperature (GMST) response to a doubling of atmospheric CO_2. ECS measures the GMST increase at equilibrium following a doubling of CO_2 relative to the preindustrial period, whereas TCR represents the GMST change at the time of CO_2 doubling under a 1% per year increase in CO_2, reflecting the transient response of the climate system[1]. Better understanding the physical processes and model characteristics that influence ECS and TCR is crucial for assessing the pace and amplitude of human-induced warming and for informing effective mitigation and adaptation strategies. Despite continuous advances in model development, large uncertainties in model-based estimates of ECS and TCR have persisted over the past few decades, including the most recent CMIP6[1].

From the classical forcing-feedback-response perspective, climate sensitivity can be influenced by either external forcing or internal climate feedback, broadly defined. The proposed candidates include, for example, cloud feedback[2,3,4,5,6,7,8,9], efficacy of radiative forcings[10], ocean heat uptake[11,12], and warming pattern[13,14]. These factors are not mutually exclusive. In parallel, another group of studies aims to relate climate sensitivity to the climatological mean state[15,16,17]. Recently, SO mean-state SST[18,19] and sea ice extent[20] are suggested to be linked to low cloud feedback and thus modulate climate sensitivity.

Accurately simulating the historical climate states, both the mean and the change, is a necessary, albeit not sufficient, condition to qualify a model for reliable future projection. Not surprisingly, climate models with a higher ECS or TCR tend to simulate a stronger anthropogenic warming rate in the historical period, suggesting an inherent link between these climate sensitivity metrics and the historical warming[21]. Understanding and constraining the inter-model spread in the historical warming rate, the aim of this study, is therefore essential for improving projections of future warming.

The historical warming rate in observations or any individual model simulation is affected by both internal climate variability and externally forced climate response, while ECS or TCR by definition only quantifies the latter. To reconcile this, initial-condition LE simulations with a given model are designed to separate the forced climate response from internal climate variability[22]. The ensemble mean of LE historical simulations reflects only the externally forced climate response, while for each ensemble member the residual after the removal of ensemble mean isolates the internal climate variability. As we will show later, the usage of LE simulations is critical if one aims to investigate the true, externally forced warming rate for the historical period in models.

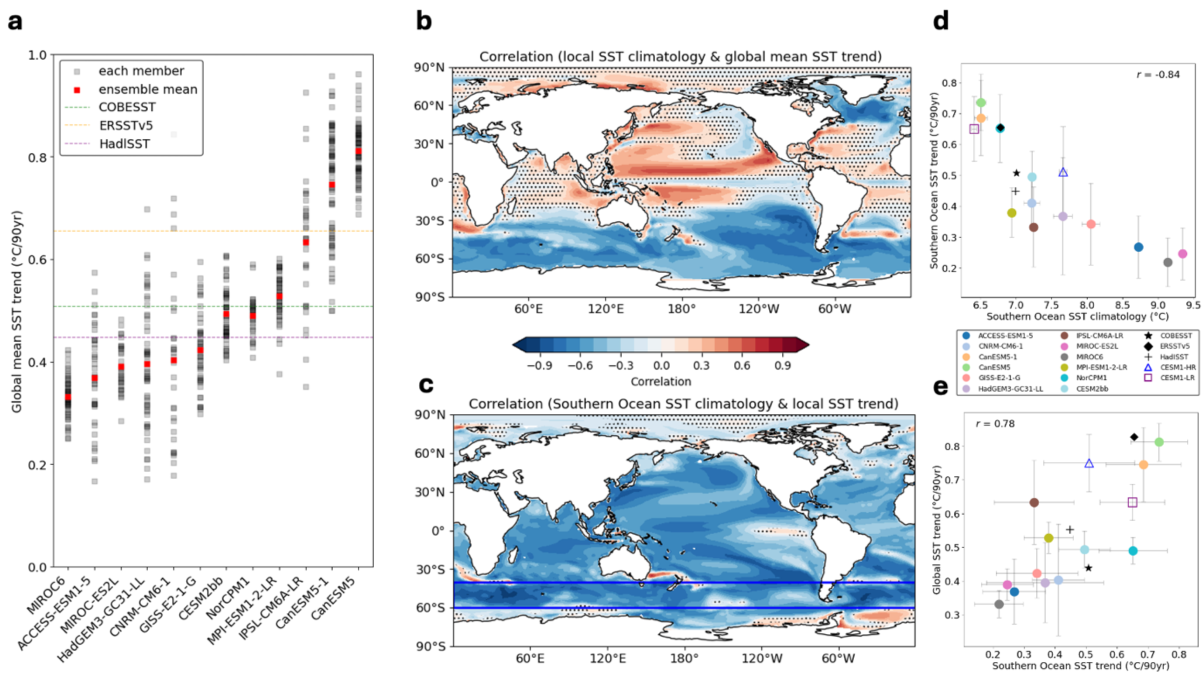

__Figure 1. Southern Ocean (SO) climatological sea surface temperature (SST) constrains historical warming. a,__ Historical global mean SST trend (1925-2014) from 12 large-ensemble (LE) models (≥30 members each). Grey squares show individual ensemble members and red squares denote ensemble means. Observational SSTs are shown as dashed horizontal lines. __b,__ Inter-model correlation between local SST climatology (1850-1920) and global mean SST trend (1925-2014) for the 12 LE models based on ensemble means. Stippling marks areas where the correlation is insignificant at the 95% confidence level, according to a two-sided Student's t-test. __c,__ As in __b__, but for the correlation between SO (40°S-60°S; highlighted with a blue box) SST climatology and SST trend at each ocean grid. __d,__ Relation between SO SST climatology and SO SST trend across models. __e,__ Relation between SO SST trend and global mean SST trend across models. In panels __d__ and __e__, uncertainty bars denote one inter-member standard deviation, and r indicates the Pearson correlation coefficient for the 12 LE models. Observations are also included in panel __d__ and __e__ for comparison.

Model disagreement in the historical warming rate

30 models in total from the CMIP6 archive are analyzed, each with at least 5 ensemble members (Methods; SI Table 1). Most of our analysis is focused on the 12 LE models that have at least 30 ensemble members each. Within a single model, the global mean sea surface temperature (GMSST) trend or the GMST trend during a 90-year historical period (1925-2014) can differ by up to a factor of 4 among the ensemble members, highlighting a strong role of internal variability (Fig. 1a). Indeed, the historical GMSST trend due to internal variability can reach up to 60% of the externally forced trend. Therefore, if one or only a few realizations of each model is used, the large inter-model spread of historical climate trends could be largely affected by internal variability.

Similarly, there is also a large spread in the ensemble-mean (i.e. forced) GMSST trend across the 12 LE models, ranging from 0.35°C to 0.82°C per 90 years (Fig. 1a). A similar conclusion can be drawn for GMST trends as the two are highly correlated (Extended Data Fig. 1). For comparison, the observed GMSST trend is 0.54°C per 90 years on average across 3 datasets (see Methods). Taken together, climate models differ by more than a factor of 2 in their simulated forced historical GMSST warming rates, an amount which is significantly larger than the observational uncertainty of trends across different datasets (0.45-0.66°C per 90 years). These model uncertainties in the simulated forced historical warming rate reflect true inter-model discrepancies not resultant from internal variability, given the large ensemble sizes for each model LE.

Tracing the uncertainties to the Southern Ocean

Motivated by previous studies[15,16,17], we investigate the possibility that the inter-model spread of forced historical warming among the CMIP6 LE models can be traced to the climatological mean state. We firstly compute the inter-model correlation between the ensemble-mean historical GMSST trend during 1925-2014 and the ensemble-mean climatological SST locally at each ocean grid averaged over a prior period, 1850-1920. Robust negative correlations are identified in almost the entire SO (Fig. 1b). Models with a cooler SO mean state tend to simulate a stronger historical GMSST warming (also see Extended Data Fig. 2), thus implying a higher climate sensitivity. In fact, the climatological SST in the SO exhibits a particularly large inter-model spread (6-10°C across 12 LE models), and two-thirds of the 12 LE models have an anomalously warm SO compared to observations[23,24,25,26] (Fig. 1d; Extended Data Fig. 2). Negative correlations are also seen in the subpolar North Atlantic but much more confined in space (Fig. 1b). Tropical ocean climatological SST is positively correlated with the historical GMSST trend, with pronounced positive correlations on either side of the equator in the western and central tropical Pacific and to a weaker extent also in the tropical Atlantic (Fig. 1b). Whether these positive correlations indicate a physical link between the tropical ocean climatological SST and the ensemble-mean historical GMSST trend or partly reflect the SO-tropical ocean connection in climatological SST (Extended Data Fig. 3) warrants further investigation. Regardless, the inter-model spread of climatological SST is relatively small in the off-equatorial regions of the west/central tropical Pacific compared to the SO (Extended Data Fig. 4). Thus, we focus on the SO for the remainder of this study.

How might the inter-model spread in climatological SST in the SO be linked to the spread in GMSST trend? Although the correlations identified here do not necessarily imply causality, previous studies on the teleconnected impacts of the SO suggest that a mechanistic explanation, beyond merely statistical, is possible. In particular, SO SST anomalies have been shown to influence surface winds over the southeastern subtropical Pacific, altering the local mixed layer heat budget via the wind-evaporation-cloud-SST feedback mechanism[12,27,28]. The resulting subtropical SST anomalies can then extend into the deep tropics via coupled ocean-atmosphere processes, impacting atmospheric deep convection and associated Rossby Wave teleconnections to the Northern Hemisphere[12,28,29,30,31].It is thus reasonable to speculate that the SO climatological SST first modulates the local SST trend, which in turn impacts the GMSST trend through the teleconnection pathways mentioned above. This conjecture is supported by the negative correlation between local SO climatological SST and SST trend (r = -0.84 for 12 LE models; Fig. 1d) and the positive correlation between the SO SST trend and GMSST trend (r = 0.78 for 12 LE models; Fig. 1e); we note that the latter correlation remains strong when the SO region is excluded from the GMSST calculation (r = 0.69). These conclusions remain valid when the analysis is expanded to the 30 climate models with smaller ensemble sizes (Extended Data Fig. 5). Furthermore, the SO climatological SST is negatively correlated with the SST trend nearly everywhere except the Arctic, equatorial eastern Pacific and Antarctic coastal regions (e.g., Weddell Sea, Amundsen Sea, and Bellingshausen Sea) (Fig. 1c). Nevertheless, it remains elusive why the SO SST trend is negatively correlated with the SO climatological SST. To elucidate this potential linkage, in the next section we will focus on the SO and quantify the contribution of the SO climatological SST to the inter-model spread in the SO forced historical warming, ranging from 0.22 K to 0.74 K per 90 years across the 12 LEs (Fig. 1d).

Modulating effect of Southern Ocean climatological SST on local warming

The mixed layer heat budget for the SO SST change in the historical period can be written as:

$$C\frac{dT}{dt} = Q_{net} - D_o \tag{1}$$

where C is the ocean mixed layer heat capacity, T is SST, $Q_{net} \approx F - \lambda_a T$ is the net ocean surface heat flux consisting of radiative forcing (F) and net surface climate feedback ($-\lambda_a T$), and D_o is the divergence of ocean heat transport. For an ocean mixed layer depth of 100 m (Extended Data Fig. 6) and an SST change of 0.44°C during 1925-2014 averaged across the 12 LEs (Fig. 1d), $C\, dT/dt$ is estimated to be 0.06 W/m^2, an order of magnitude smaller than CO_2-induced radiative forcing for this period (0.96 W/m^2; Methods). This implies a quasi-equilibrium state under a slowly evolving, transient climate in which $Q_{net} \approx D_o$, as also reported by previous studies[32]. In a two-ocean layer conceptual framework[33], D_o is often parameterized as $\lambda_o(T - T_d)$ where the deep ocean temperature change T_d is relatively small for short-term changes. Taken together, it leads us to derive that,

$$T \approx \frac{F}{\lambda} \equiv \frac{F}{\lambda_a + \lambda_o} \tag{2}$$

where λ is the effective surface climate feedback that includes contributions from both the net surface heat flux-induced atmospheric damping (λ_a) and the ocean heat transport-induced damping (λ_o). According to Eq. (2), the inter-model spread in SO SST change over the period 1925-2014 is determined by the radiative forcing (F) and the effective surface climate feedback

(λ). These two factors will be discussed below firstly for the multi-model mean across the 12 LE models and then for the inter-model spread with connections to the climatological SST.

During 1925-2014, atmospheric CO_2 is the dominant radiative forcing agent in the SO, although other forcing agents may play a significant role in certain periods (e.g., ozone forcing after the 1970s[34]. Here we focus on the CO_2 -induced radiative forcing in our analysis of F. Using an offline radiative transfer model, we estimate that the radiative forcing F due to the CO_2 increase during 1925-2014 (from 305 to 400 ppm) is 0.96 W m^{-2} (Methods). The forced SO SST change T during 1925-2014 is 0.44 K on average across the LEs. Utilizing Eq. (2), we can estimate that the effective surface climate feedback λ is 2.18 W m^{-2} K^{-1}.

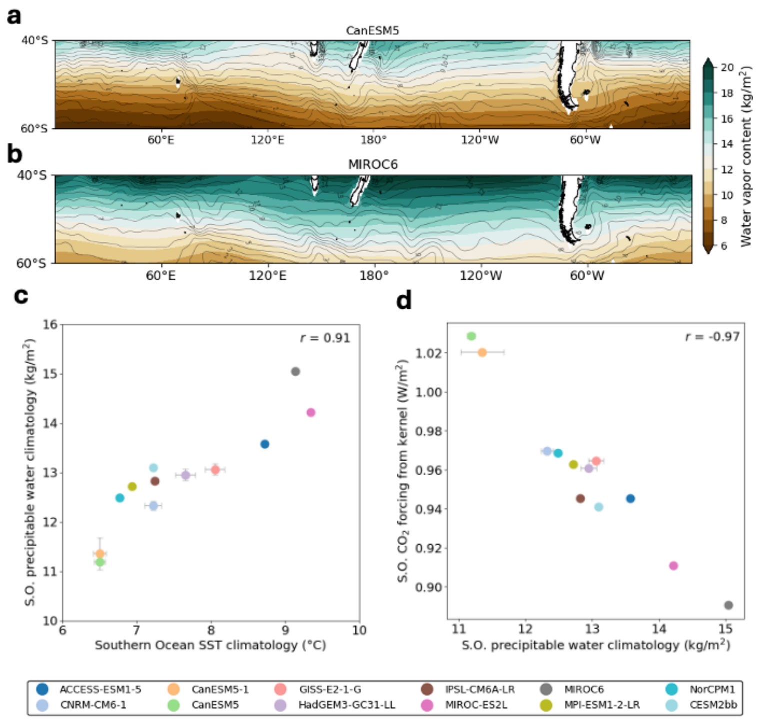

Figure 2. State dependence of CO_2 surface radiative forcing. *Mechanism linking CO_2-induced surface downward longwave radiative forcing in clear sky (rldscs) to climatological atmospheric water vapor content (prw).* ***a,*** *Climatological sea surface temperature (SST; contours at 1 °C interval) overlaid on climatological precipitable water (shading) for CanESM5.* ***b,*** *As in a, but for MIROC6.* ***c,*** *Relation between Southern Ocean (SO; 40°S-60°S) SST climatology and SO climatological precipitable water across models.* ***d,*** *Relation between SO climatological precipitable water and SO historical (1925-2014) CO_2-induced surface clear-sky longwave radiative flux (downward positive) from the offline radiative calculation (Methods). In panels* ***c*** *and* ***d****, uncertainty bars denote one inter-member standard deviation, and r indicates the Pearson correlation coefficient.*

How do these determining factors, F and λ, differ across climate models? Are they dependent on climatological SST? As CO_2 increases, the atmospheric emissivity increases, which therefore enhances the downwelling longwave radiative flux reaching the surface. In models with a warmer climatological SST, the warmer atmosphere contains more precipitable water following the Clausius-Clapeyron relation (Fig. 2a-c; Extended Data Fig. 7), and the increase of atmospheric emissivity due to the increased CO_2 is less effective for an already opaque atmosphere. Although the negative correlation between climatological precipitable water and surface downwelling clear-sky longwave radiative flux (Extended Data Fig. 8) is consistent with this argument, an apparent caveat exists: the diagnosed increase in downward longwave radiative flux also includes the temperature increase effect. To reconcile this, offline radiative calculations of CO_2 increase are conducted for each LE model separately with its own vertical profiles of climatological temperature and humidity over the SO (Methods). Based on these calculations, models with more precipitable water indeed have a weaker CO_2 surface radiative forcing (r = -0.97), although the forcing (F) spread [0.89 W m^{-2}, 1.02 W m^{2}] is relatively small (Fig. 2d). Substituting the F spread into Eq. (2) yields a corresponding T spread of [0.41 K, 0.47 K], which explains about 12% of the total T spread [0.22 K, 0.74 K] across the 12 LEs.

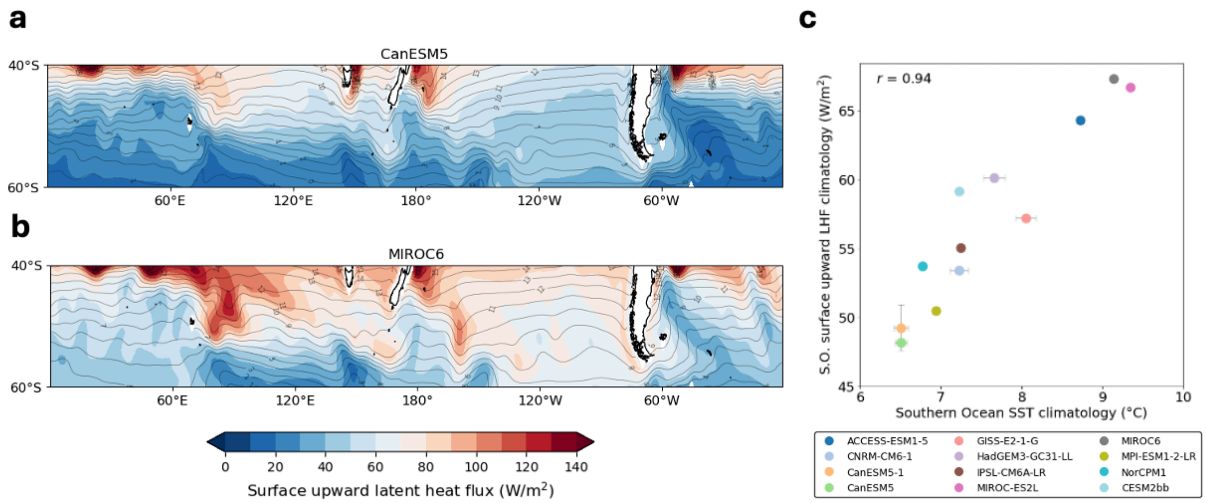

Figure 3. State dependence of evaporative damping effect. ***a****, Climatological sea surface temperature (SST; contours at 1 °C interval) overlaid on surface latent heat flux climatology (upward positive; shadings) for CanESM5.* ***b****, As in* ***a****, but for MIROC6.* ***c****, Relation between Southern Ocean (40°S-60°S; SO) SST climatology and SO climatological surface latent heat flux across the ensemble means of the 12 LE models. In panel* ***c****, uncertainty bars denote one inter-model standard deviation, and* r *indicates the Pearson correlation coefficient.*

The effective climate feedback consists of the contribution from both atmospheric damping (λ_a) and oceanic damping (λ_o), and the former further consists of four components ($\lambda_a = \lambda_{SW} + \lambda_{LW} + \lambda_{SH} + \lambda_{LH}$) including the surface shortwave and longwave radiative fluxes, sensible and latent heat fluxes, respectively. Among them, the evaporative damping feedback (λ_{LH}) is directly modulated by the climatological SST[32]. Latent heat flux can be approximated as, $LH \approx \rho_{air} L_v C_E W q^*(1 - \mathcal{H})$, where ρ_{air} is air density, L_v is latent heat of vaporization, C_E is transfer coefficient, W is surface wind speed, $\mathcal{H}$ is relative humidity, and q^* is saturation specific humidity exponentially dependent on SST (i.e., Clausius-Clapeyron relation). Therefore, we have,

$$\lambda_{LH} \equiv \frac{\partial LH}{\partial T} \approx \alpha \overline{LH} \qquad (3)$$

constrained by the climatological latent heat flux (denoted by the overbar) and the parameter $\alpha \approx$ 0.07 K^{-1} from the Clausius-Clapeyron relation. Models with a warmer climatological SST tend to have a higher climatological latent heat flux in the SO (r = 0.94 for 12 LE models), the difference of which can reach as large as 19 W m^{-2} between the warmest and coldest models (Fig. 3; also see Extended Data Fig. 9). Based on Eq. (3), λ_{LH} can thus differ by 1.33 $W\ m^{-2}\ K^{-1}$ across the 12 LE models, which is substantial compared to the multi-model mean value of λ, 2.18 W m^{-2} K^{-1}. Allowing λ to vary over the range of [1.51 W m^{-2} K^{-1}, 2.84 W m^{-2} K^{-1}], we estimate the T spread due to the SST-dependent λ_{LH} spread to be [0.34 K, 0.64 K], which explains about 58% of the total T spread [0.22 K, 0.74 K].

Taken together, our theoretical estimate suggests that the LE spread of climatological SST in the SO can explain at least 70% of the spread of the local forced historical SST trend, 12% from CO_2-induced radiative forcing and 58% from warming-induced evaporative damping.

Finally, we briefly discuss other possible mechanisms that are potentially related to climatological SST. Ocean mixed layer depth, which determines the heat capacity C in Eq. (1), varies by ~40% across the models investigated, and its relation with climatological SST is insignificant (Extended Data Fig. 6). Also, its influence on the spread of SO SST trends should be small, given that the temperature tendency term is an order of magnitude smaller than the CO_2-induced radiative forcing in Eq. (1). A cooler SO is found to be associated with a greater Antarctic sea ice extent (Extended Data Fig. 10) and thus a larger 'capacity of change'[18], which can potentially favor stronger ice albedo feedback further mediated by low cloud changes[20]. But the state dependence of this feedback loop involving ice extent has yet to be rigorously demonstrated and is hard directly quantify without targeted numerical experiments. We have also attempted to investigate the inter-model relation between climatological SST and cloud-related quantities, as cloud feedback is known to be important for the SO climate[6,8]. However, no statistically significant relationships have been identified for any of the cloud-related variables investigated, including climatological cloud area fraction, liquid water path, ice water path, cloud-induced surface shortwave and longwave radiative fluxes (Extended Data Fig. 11). Upper ocean salinity has been proposed to influence ocean stratification and, consequently, the rate of SO surface warming[35]. However, this mechanism is not evident in our analysis: climatological sea surface salinity is neither correlated with the climatological SST nor correlated with the historical SST trend in the SO across the 12 LEs (Extended Data Fig. 12).

Discussion

Based on the 12 LE models (each having at least 30 members) in the CMIP6 archive, we find a large (factor of 2 to 3) inter-model spread in the magnitude of forced global warming over the historical period 1925-2014, which we suggest may be partially attributable to the spread of climatological SO SST. Models with a climatologically warmer SO tend to simulate a weaker SO SST warming, which potentially contributes to a weaker GMSST warming through teleconnections. Two mechanisms are proposed to explain the state dependence of SO surface warming, and theoretical quantifications are further provided. First, a warmer SO is associated with a warmer, moister atmosphere that acts to suppress the surface longwave radiative forcing induced by a certain increase of atmospheric CO_2. Second, a warmer SO is associated with a larger latent heat flux that acts to enhance the evaporative damping effect. These two SO climatological SST-dependent mechanisms together can explain 70% of the model spread of SO warming, 12% through the CO_2 forcing and 58% through the evaporative damping. Including all 30 CMIP6 models (18 of which have ensemble sizes between 5-29 members) yields overall consistent results.

Complementing the existing literature with various proposed approaches[4,6,10,14,35,36,37,38], our study provides another possible candidate to constrain ECS with the SO climatological SST, with clear theoretical support beyond purely statistical relations. For the historical period, the observational records fall well within the inter-model relation between the SO ensemble-mean climatological SST and the SO ensemble-mean historical SST trend across the 12 LEs, validating our methodology (Fig. 1d; Extended Data Fig. 5).

Our study highlights an urgent need for reducing the SO climatological SST bias and narrowing its inter-model spread (Fig. 1d; Extended Data Fig. 4) in order to improve the SO SST response to external forcing. To illustrate this opportunity, we analyze the Community Earth System Model version 1 (CESM1) historical simulations (10 members each) in its low-resolution (LR) and high-resolution (HR) configurations[39]. Compared to CESM1-LR, CESM1-HR has a warmer SO climatological SST and a weaker SO historical warming, consistent with the relation identified for the CMIP6 model ensemble (Fig. 1d, Extended Data Fig. 5). More targeted model experiments with a modified SO climatological SST are now underway to explicitly test its influence on the historical warming in the SO and the globe.

Methods

Observational datasets

Three monthly observational SST datasets are used: (1) National Oceanic and Atmospheric Administration Extended Reconstructed Sea Surface Temperature Version 5 (ERSSTv5) with a resolution of 2° × 2°[40]. (2) Hadley Centre Sea Ice and SST v.1.1 (HadISST 1.1) with a resolution of 1° × 1°[41]. (3) Centennial In Situ Observation-Based Estimates of the Variability of SST and Marine Meteorological Variables (COBE) with a resolution of 1° × 1°[42]. For consistency across datasets and comparability with model outputs, all SST products are regridded to a resolution of 1° × 1°.

CMIP6 LE simulations

We use historical all-forcing simulations from the CMIP6 archive (Supplementary Table S1). A total of 30 CMIP6 LE models are analyzed, each with at least 5 ensemble members. With SST as an example, 4 models have 5-9 members, 10 models have 10-19 members, 4 models have 20-29 members, and 12 models have more than 30 members, resulting in a total of 754 ensemble members from 30 models. The ensemble sizes of other main variables are generally comparable with SST. Detailed information on model names, ensemble sizes, and variable availability is provided in Supplementary Table S1. All the model variables are regridded to a resolution of 1° × 1° for inter-model comparison.

The primary variables analyzed include SST (tos), surface temperature (ts), atmosphere water vapor content (prw), sea-ice area percentage (siconc), ocean mixed layer depth defined by sigma T (mlotst), surface upward latent heat flux (hfls), surface downwelling shortwave flux in air (rsds), surface downwelling shortwave flux in air assuming clear sky (rsdscs), surface downwelling longwave flux in air (rlds), surface downwelling longwave flux in air assuming clear sky (rldscs), atmosphere cloud condensed water content (clwvi), atmosphere cloud ice content (clivi), and cloud area fraction (clt).

CESM1 simulations

CESM v1.3 with high-resolution and low-resolution (CESM1-HR, CESM1-LR) configurations were analyzed. Both models contain 10 ensemble members. For the historical trend analysis, years 1925-2005 are from the historical simulations, and years 2006-2014 are from the RCP8.5 simulations. CESM1-LR has a resolution of 1° × 1° for all components. CESM1-HR has a resolution of 0.25° × 0.25° for atmosphere and land models and 0.1° × 0.1° for the ocean and sea-ice models. Surface temperature is used for comparison with SST in CMIP6 simulations.

Definitions

In this study, the SO is defined as the region spanning 40°S to 60°S. The climatological mean state is calculated over the period 1850–1920, while the historical linear trend is computed over a subsequent 90-year period 1925-2014. The two time periods are chosen to be non-overlapping to ensure that the mean state and trend metrics remain independent and do not influence each other. All the results presented are based on annual averages.

Statistical significance

To assess the robustness of our results, we conduct significance tests throughout the study using the two-tailed Student's *t*-test. Statistical significance is evaluated at the 95% confidence level unless otherwise specified. This approach is applied to determine whether the diagnosed differences or trends are unlikely to occur by random chance, thereby enhancing the reliability of the reported findings.

CO_2-induced downward surface longwave radiative forcing from the offline radiative transfer model

CO_2-induced downward surface longwave radiative forcing employed to test the causal hypothesis was obtained by taking the difference between two sets of clear-sky downward longwave radiations at the surface (rldscs). They were calculated using a versatile offline radiative transfer model widely used in the atmospheric radiation community, MODTRAN 5.2[43]. For the first set of calculations, the inputs to MODTRAN 5.2 are the mean-state water vapor and temperature profiles as well as surface temperature climatology from each individual model simulation, respectively. CO_2 concentration is set to be 305 ppm, and other trace gases are from the default typical profiles included in MODTRAN 5.2[44]. The inputs to the second set are the same as the first one except for the CO_2 concentration being instantaneously increased by 31%, i.e., approximately the historical rise from 305 ppm to 400 ppm between 1925 and 2014. The differences in rldscs between the two sets thus reflect only the direct effect of CO_2, excluding feedback processes.

Data Availability

All data used in this study are available online. For observational datasets, the NOAA's ERSSTv5 data are available at https://psl.noaa.gov/data/gridded/data.noaa.ersst.v5.html; HadISST 1.1 data at https://www.metoffice.gov.uk/hadobs/hadisst/data/download.html; COBE SST at https://psl.noaa.gov/data/gridded/data.cobe.html. For model simulations, CMIP6 data are available at: https://aims2.llnl.gov/search; CESM1-HR and CESM1-LR data are available through the Casper cluster at /glade/campaign/collections/cmip/CMIP6/CESM-HR/CVDP/archive_remapped/.

Acknowledgments

Y.T. was supported in part by the National Science Foundation (NSF) National Center for Atmospheric Research (NCAR) Graduate Visitor Program during summer 2025. NSF-NCAR is a major facility sponsored by the NSF under Cooperative Agreement No. 1755088. Any opinions, findings and conclusions, or recommendations expressed in this material do not necessarily reflect the views of the National Science Foundation. We thank Ivy Tan, Jiang Zhu, Yue Dong, Yen-Ting Hwang, and Pedro DiNezio, and Yan Pan for helpful discussions and comments.

Author contributions

S. H. conceived the study. Y. T. performed the data analysis and wrote the first draft of the paper. X. C. and X. H. conducted the offline radiative calculation. All authors contributed to the interpretation of the results and refinement of the paper.

Competing interests

The authors declare no competing interests.

Additional information

Correspondence and requests for materials should be addressed to Shineng Hu.

References

1. Forster, P., T. Storelvmo, K. Armour, W. Collins, J.-L. Dufresne, D. Frame, D.J. Lunt, T. Mauritsen, M.D. Palmer, M. Watanabe, M. Wild, and H. Zhang, 2021: The Earth's Energy Budget, Climate Feedbacks, and Climate Sensitivity. In Climate Change 2021: The Physical Science Basis. Contribution of Working Group I to the Sixth Assessment Report of the Intergovernmental Panel on Climate Change [Masson-Delmotte, V., P. Zhai, A. Pirani, S.L. Connors, C. Péan, S. Berger, N. Caud, Y. Chen, L. Goldfarb, M.I. Gomis, M. Huang, K. Leitzell, E. Lonnoy, J.B.R. Matthews, T.K. Maycock, T. Waterfield, O. Yelekçi, R. Yu, and B. Zhou (eds.)]. Cambridge University Press, Cambridge, United Kingdom and New York, NY, USA, pp. 923–1054, doi:10.1017/9781009157896.009.
2. Cess, R. D., Potter, G. L., Blanchet, J. P., Boer, G. J., Ghan, S. J., Kiehl, J. T., ... & Yagai, I. (1989). Interpretation of cloud-climate feedback as produced by 14 atmospheric general circulation models. Science, 245(4917), 513-516.
3. Fasullo, J. T., & Trenberth, K. E. (2012). A less cloudy future: The role of subtropical subsidence in climate sensitivity. *science*, *338*(6108), 792-794.
4. Sherwood, S. C., Bony, S., & Dufresne, J. L. (2014). Spread in model climate sensitivity traced to atmospheric convective mixing. Nature, 505(7481), 37-42.
5. Stevens, B., Sherwood, S. C., Bony, S., & Webb, M. J. (2016). Prospects for narrowing bounds on Earth's equilibrium climate sensitivity. Earth's Future, 4(11), 512-522.
6. Tan, I., Storelvmo, T., & Zelinka, M. D. (2016). Observational constraints on mixed-phase clouds imply higher climate sensitivity. *Science*, *352*(6282), 224-227.
7. Knutti, R., Rugenstein, M. A., & Hegerl, G. C. (2017). Beyond equilibrium climate sensitivity. Nature Geoscience, 10(10), 727-736.
8. Myers, T. A., Scott, R. C., Zelinka, M. D., Klein, S. A., Norris, J. R., & Caldwell, P. M. (2021). Observational constraints on low cloud feedback reduce uncertainty of climate sensitivity. Nature Climate Change, 11(6), 501-507.
9. Wang, C., Yang, W., Vecchi, G., Zhang, B., Soden, B. J., & Chan, D. (2025). Diagnosing the factors that contribute to the intermodel spread of climate feedback in CMIP6. Journal of climate, 38(3), 663-674.
10. Marvel, K., Schmidt, G. A., Miller, R. L., & Nazarenko, L. S. (2016). Implications for climate sensitivity from the response to individual forcings. Nature Climate Change, 6(4), 386-389.
11. Winton, M., Takahashi, K., & Held, I. M. (2010). Importance of ocean heat uptake efficacy to transient climate change. Journal of Climate, 23(9), 2333-2344.
12. Hu, S., Xie, S. P., & Kang, S. M. (2022). Global warming pattern formation: The role of ocean heat uptake. Journal of Climate, 35(6), 1885-1899.
13. Armour, K. C., Bitz, C. M., & Roe, G. H. (2013). Time-varying climate sensitivity from regional feedbacks. Journal of Climate, 26(13), 4518-4534.
14. Dong, Y., Armour, K. C., Zelinka, M. D., Proistosescu, C., Battisti, D. S., Zhou, C., & Andrews, T. (2020). Intermodel spread in the pattern effect and its contribution to climate sensitivity in CMIP5 and CMIP6 models. *Journal of Climate*, *33*(18), 7755-7775.
15. Caballero, R., & Huber, M. (2013). State-dependent climate sensitivity in past warm climates and its implications for future climate projections. Proceedings of the National Academy of Sciences, 110(35), 14162-14167.

16. Anagnostou, E., John, E. H., Babila, T. L., Sexton, P. F., Ridgwell, A., Lunt, D. J., ... & Foster, G. L. (2020). Proxy evidence for state-dependence of climate sensitivity in the Eocene greenhouse. Nature communications, 11(1), 4436.
17. Zhu, J., Poulsen, C. J., & Tierney, J. E. (2019). Simulation of Eocene extreme warmth and high climate sensitivity through cloud feedbacks. Science advances, 5(9), eaax1874.
18. Kajtar, J. B., Santoso, A., Collins, M., Taschetto, A. S., England, M. H., & Frankcombe, L. M. (2021). CMIP5 intermodel relationships in the baseline Southern Ocean climate system and with future projections. *Earth's Future*, *9*(6), e2020EF001873.
19. Shin, S. J., Yeh, S. W., An, S. I., Keenlyside, N., Xie, S. P., & Park, J. H. (2023). Southern ocean control of 2°C global warming in climate models. *Earth's Future*, *11*(1), e2022EF003212.
20. Vogt, L., de Lavergne, C., Sallée, J. B., Kwiatkowski, L., Frölicher, T. L., & Terhaar, J. (2025). Increased future ocean heat uptake constrained by Antarctic sea ice extent. Earth System Dynamics, 16(5), 1453-1482.
21. Tokarska, K. B., Stolpe, M. B., Sippel, S., Fischer, E. M., Smith, C. J., Lehner, F., & Knutti, R. (2020). Past warming trend constrains future warming in CMIP6 models. *Science advances*, *6*(12), eaaz9549.
22. Deser, C., Lehner, F., Rodgers, K. B., Ault, T., Delworth, T. L., DiNezio, P. N., ... & Ting, M. (2020). Insights from Earth system model initial-condition large ensembles and future prospects. *Nature Climate Change*, *10*(4), 277-286.
23. Wang, C., Zhang, L., Lee, S. K., Wu, L., & Mechoso, C. R. (2014). A global perspective on CMIP5 climate model biases. *Nature Climate Change*, *4*(3), 201-205.
24. Hyder, P., Edwards, J. M., Allan, R. P., Hewitt, H. T., Bracegirdle, T. J., Gregory, J. M., ... & Belcher, S. E. (2018). Critical Southern Ocean climate model biases traced to atmospheric model cloud errors. Nature communications, 9(1), 3625.
25. Schuddeboom, A. J., & McDonald, A. J. (2021). The Southern Ocean radiative bias, cloud compensating errors, and equilibrium climate sensitivity in CMIP6 models. *Journal of Geophysical Research: Atmospheres*, *126*(22), e2021JD035310.
26. Luo, F., Ying, J., Liu, T., & Chen, D. (2023). Origins of Southern Ocean warm sea surface temperature bias in CMIP6 models. *npj Climate and Atmospheric Science*, *6*(1), 127.
27. Hwang, Y. T., & Frierson, D. M. (2013). Link between the double-Intertropical Convergence Zone problem and cloud biases over the Southern Ocean. Proceedings of the National Academy of Sciences, 110(13), 4935-4940.
28. Kim, H., Kang, S. M., Kay, J. E., & Xie, S. P. (2022). Subtropical clouds key to Southern Ocean teleconnections to the tropical Pacific. Proceedings of the National Academy of Sciences, 119(34), e2200514119.
29. Zhang, X., Deser, C., & Sun, L. (2021). Is there a tropical response to recent observed Southern Ocean cooling?. Geophysical Research Letters, 48(5), e2020GL091235.
30. Dong, Y., Armour, K. C., Battisti, D. S., & Blanchard-Wrigglesworth, E. (2022). Two-way teleconnections between the Southern Ocean and the tropical Pacific via a dynamic feedback. Journal of Climate, 35(19), 6267-6282.
31. Kang, S. M., Yu, Y., Deser, C., Zhang, X., Kang, I. S., Lee, S. S., ... & Ceppi, P. (2023). Global impacts of recent Southern Ocean cooling. Proceedings of the National Academy of Sciences, 120(30), e2300881120.

32. Xie, S. P., Deser, C., Vecchi, G. A., Ma, J., Teng, H., & Wittenberg, A. T. (2010). Global warming pattern formation: Sea surface temperature and rainfall. Journal of Climate, 23(4), 966-986.
33. Held, I. M., Winton, M., Takahashi, K., Delworth, T., Zeng, F., & Vallis, G. K. (2010). Probing the fast and slow components of global warming by returning abruptly to preindustrial forcing. Journal of Climate, 23(9), 2418-2427.
34. Liu, W., Hegglin, M. I., Checa-Garcia, R., Li, S., Gillett, N. P., Lyu, K., ... & Swart, N. C. (2022). Stratospheric ozone depletion and tropospheric ozone increases drive Southern Ocean interior warming. Nature Climate Change, 12(4), 365-372.
35. Liu, M., Soden, B. J., Vecchi, G. A., & Wang, C. (2023). The spread of ocean heat uptake efficiency traced to ocean salinity. Geophysical research letters, 50(4), e2022GL100171.
36. Cox, P. M., Huntingford, C., & Williamson, M. S. (2018). Emergent constraint on equilibrium climate sensitivity from global temperature variability. Nature, 553(7688), 319-322.
37. Schmittner, A., Urban, N. M., Shakun, J. D., Mahowald, N. M., Clark, P. U., Bartlein, P. J., ... & Rosell-Melé, A. (2011). Climate sensitivity estimated from temperature reconstructions of the Last Glacial Maximum. Science, 334(6061), 1385-1388.
38. Merlis, T. M., Held, I. M., Stenchikov, G. L., Zeng, F., & Horowitz, L. W. (2014). Constraining transient climate sensitivity using coupled climate model simulations of volcanic eruptions. Journal of Climate, 27(20), 7781-7795.
39. Chang, P., Zhang, S., Danabasoglu, G., Yeager, S. G., Fu, H., Wang, H., ... & Wu, L. (2020). An unprecedented set of high‐resolution earth system simulations for understanding multiscale interactions in climate variability and change. Journal of Advances in Modeling Earth Systems, 12(12), e2020MS002298.
40. Huang, B., Thorne, P. W., Banzon, V. F., Boyer, T., Chepurin, G., Lawrimore, J. H., ... & Zhang, H. M. (2017). Extended reconstructed sea surface temperature, version 5 (ERSSTv5): upgrades, validations, and intercomparisons. Journal of Climate, 30(20), 8179-8205.
41. Rayner, N. A., Parker, D. E., Horton, E. B., Folland, C. K., Alexander, L. V., Rowell, D. P., ... & Kaplan, A. (2003). Global analyses of sea surface temperature, sea ice, and night marine air temperature since the late nineteenth century. Journal of Geophysical Research: Atmospheres, 108(D14).
42. Ishii, M., Shouji, A., Sugimoto, S. & Matsumoto, T. Objective analyses of sea-surface temperature and marine meteorological variables for the 20th century using ICOADS and the Kobe collection. Int. J. Climatol. 25, 865–879 (2005).
43. Berk, A., Anderson, G. P., Acharya, P. K., Bernstein, L. S., Muratov, L., Lee, J., ... & Lewis, P. E. (2005, June). MODTRAN 5: a reformulated atmospheric band model with auxiliary species and practical multiple scattering options: update. In *Algorithms and technologies for multispectral, hyperspectral, and ultraspectral imagery XI* (Vol. 5806, pp. 662-667). SPIE.
44. McClatchey, R., R. W. Fenn, J.E.A. Selby, F.E. Volz, JS. Garing (1972). Optical properties of the atmosphere (Third Edition), AFCLR-72-0497, Air Force Cambridge Research Laboratories, Environmental Research Papers, No. 411.